Plasma Chem Plasma Process (2012) 32:495–518
DOI 10.1007/s11090-012-9365-0

ORIGINAL PAPER

Thermophysical Properties of High Temperature Reacting Mixtures of Carbon and Water in the Range 400–30,000 K and 0.1–10 atm. Part 2: Transport Coefficients

WeiZong Wang · J. D. Yan · MingZhe Rong · A. B. Murphy · J. W. Spencer

Received: 10 November 2011 / Accepted: 28 December 2011 / Published online: 29 March 2012

Abstract The present contribution is continuation of Part 1: Equilibrium composition and thermodynamic properties. This paper is devoted to the calculation of transport properties of mixtures of water and carbon at high temperature. The transport properties, including electron diffusion coefficient, viscosity, thermal conductivity, and electrical conductivity are obtained by using the Chapman–Enskog method expanded to the third-order approximation (second-order for viscosity), taking only elastic processes into account. The calculations, which assume local thermodynamic equilibrium, are performed for atmospheric pressure plasmas in the temperature range from 400 to 30,000 K for pressures of 0. 10, 1.0, 3.0, 5.0 and 10.0 atm. with the results obtained are compared to those of previously published studies, and the reasons for discrepancies are analyzed. The results provide reliable reference data for simulation of plasmas in mixtures of carbon and water.

Keywords Carbon · Water · Thermal plasmas · Chapman–Enskog method · Transport properties · Viscosity · Thermal conductivity · Electrical conductivity · Diffusion coefficient

W. Wang · M. Rong
State Key Laboratory of Electrical Insulation and Power Equipment, Xi'an Jiaotong University, Xi'an Shaanxi 710049, People's Republic of China

W. Wang (✉) · J. D. Yan (✉) · J. W. Spencer
Department of Electrical Engineering and Electronics, The University of Liverpool, Brownlow Hill, Liverpool L69 3GJ, UK
e-mail: wangweizong@gmail.com

J. D. Yan
e-mail: yaneee@liv.ac.uk

A. B. Murphy
CSIRO Materials Science and Engineering, PO Box 218, Lindfield, NSW 2070, Australia

Introduction

In the first paper of this series, the chemical equilibrium composition and a set of thermodynamic properties including mass density, molar weight, specific enthalpy, specific entropy, specific heat at constant pressure, sonic velocity and heat capacity ratio were calculated for mixtures of carbon and water [1]. In this calculation, a large number of chemical species (69 heavy species in all) as well as electrons, including relevant atoms, ions and molecules, are taken into account: C(s), C, C^+, C^-, C_2, C_2^-, C_3, C_4, C_5, C_2^+, C^{++}, C^{+++}, H, H^+, H^-, H_2, H_2^-, H_2^+, H_3^+, O_2, O_2^-, O_2^+, O, O_3, O^+, O^{++}, O^{+++}, O^-, CH, CH_2, CH_3, CH_4, C_2H, C_3H, C_4H, C_5H, C_6H, C_2H_2, C_2H_4, CH^+, CH^-, CO, CO_2, C_2O, C_3O_2, CO^+, CO_2^+, CO^-, CO_2^-, OH, OH^+, OH^-, HO_2^+, HO_2^-, H_3O^+, H_2O_2, H_2O, H_2O^+, CH_2O, CHO, C_2H_4O, CHO^+, HCO_3^-, CH_4O, CH_2OH, CH_3O, COOH, HCOOH, C_2H_6O.

It was found that in the C–H–O system, the species composition and thus thermodynamic properties strongly depend on the admixture ratios of carbon and water steam as well as the phase transition of carbon. As the proportion of carbon increases, a greater number of species appear in appreciable concentrations in the reacting mixture, leading to a complex reaction field due to the high reactivity of C/H/O species. The equilibrium composition of the plasma has, of course, a great influence on mass, momentum and heat transfer. Calculation of the composition is a prerequisite to obtaining the plasma transport coefficients, whose calculation is described in the present paper.

Transport coefficients for mixtures of C, H and O have been presented by Aubreton et al. [2], who performed calculations for CO–H_2 plasmas and other mixtures representative of those produced by gasification of biomass. They assumed that the O/C ratio was at least 0.8, while the O/H ratio could take any value. Under this assumption, 27 species and 18 main species are respectively taken into account in the calculating the composition and transport properties including viscosity, thermal conductivity and electrical conductivity. These coefficients can be obtained for all other C\H\O mixtures wherein O/C >0.8. However, due to the carbon-rich environment near graphite electrodes, there will be situations in which the O/C ratio falls below 0.8 in carbon–water plasmas. In this case, a greater range of species has to be taken into account because of the high reactivity of C, H and O species with each other.

Tanaka et al. [3] presented transport properties for CO_2–H_2 mixtures at atmospheric pressure. Their calculation used only a first-order approximation of the Chapman–Enskog method for both electrons and heavy species, which is less reliable than calculations using higher-order approximations; typically a third-order approximation is used for electrons.

To our knowledge, no data for the transport coefficients of reacting mixtures of carbon and water can be found in the literature, especially for temperatures below 6,000 K, for which the dissociation and conversion of the neutral species dominates and carbon in the condensed state can also be present. The aim of this paper is to present a systematic study of high-temperature transport coefficients of carbon and water mixtures.

The water–carbon mixture is described by the formula $C_q(H_2O)_{1-q}$, where the carbon molar amount q was chosen to range from 0 to 1 in steps of 0.1. We assume that the plasmas are in local thermodynamic equilibrium (LTE), and present calculations of transport coefficients (namely diffusion coefficients, thermal conductivities, electrical conductivity and viscosity) of this mixture for the temperature range 400–30,000 K, conditions which can satisfy most requirements of thermal plasmas modelling. Further, the influence of solid carbon formation and pressure on the properties is also included in this paper.

The paper is organized as follows: in second section, the method of calculation of the transport coefficients is outlined. The collision integrals, the choice of intermolecular

potentials used in evaluating them and various approaches used in determining transport properties are presented in third section. Calculated transport coefficients for reacting mixtures of carbon and water with or without the formation of solid carbon, and a comparison of the calculated properties with available literature data for high temperature water steam and carbon dioxide plasmas, are given in section "Results and Comparisons". In section "Influence of Pressure on Transport Properties", the influence of pressure on transport coefficients is illustrated. Finally, conclusions are presented in last section.

Method of Calculation

Transport properties, namely diffusion coefficients, electrical conductivity, thermal conductivities and viscosity, are calculated approximately using the classical Chapman–Enskog method, which has been analyzed exhaustively in the literature [3–6]. The distribution function of the different species is assumed to be a Maxwellian with by a first-order perturbation. The first-order perturbation function is developed by means of a series of Sonine polynomials and then expressed in terms of expansion coefficients, yielding a linearization of the Boltzmann equation and leading to the introduction of systems of linear equations. The solution of these linear equations to a selected order allows the transport coefficients to be determined.

The order chosen in the approximate calculation governs the dimensions of the system of linear equations with which the distribution function and the Boltzmann equation are solved with an expansion expression [7]. The accuracy of the transport properties is improved by increasing the order. However, this requires a greater number of effective collision integrals, which are terms appearing in the expressions of the transport coefficients, and the number of calculations rapidly becomes prohibitive [8]. It has been found that at least a third-order approximation is needed at low temperatures around 5,000 K for the ordinary diffusion for interactions involving electrons [9]. The first-order approximation for viscosity can differ by more than 10 % at high temperature from the third-order approximation. It was concluded that in this case the second-order approximation was adequate [10]. Therefore, this paper utilizes the third-order approximation for transport properties except viscosity, for which the second-order approximation is considered.

For thermal conductivity, besides the translational component, the contributions from the internal energy and chemical reactions should also be taken into account. Chemical reactions (dissociation, recombination, ionization and so on) in a plasma in chemical equilibrium leads to additional heat transfer. This leads to an additional reactive thermal conductivity λ_{re}, which was studied by Butler and Brokaw for neutral gas mixtures [11]; their expressions were subsequently extended to ionized gases by Meador and Stanton [12]. The presence of internal degrees of freedom as a result of vibrational, rotational and electronic excitation can affects the heat flux vector and is included using an internal thermal conductivity λ_{in}, which has been derived using the Hirschfelder–Eucken approximation [13–15].

Collision Integrals

The transport coefficients rely on collision integrals, which take into account the pair interaction potential between two colliding species i and j. They are statistical averages

over a Maxwellian distribution of the binary collision cross sections, and are defined as follows:

$$\Omega_{ij}^{(l,s)} = \sqrt{\frac{kT}{2\pi\mu_{ij}}} \int_0^\infty \exp\left(-\gamma_{ij}^2\right) \gamma_{ij}^{2s+3} Q_{ij}^l(g) d\gamma_{ij} \tag{1}$$

The transport cross sections $Q_{ij}^l(g)$ are evaluated by

$$Q_{ij}^l(g) = 2\pi \int_0^\infty \left(1 - \cos^l \chi\right) b\, db \tag{2}$$

where the parameters μ_{ij}, χ, g and b are the reduced mass, the angle by which the molecules are deflected in the centre of gravity coordinate system, section, the relative velocity of the two particles, and the impact parameter of the colliding species i and j, respectively. The indices (l, s) are directly related to the order of approximation used for the transport coefficients. The angle of deflection depends on the intermolecular potential of the colliding species.

In the following subsections, we consider the intermolecular potentials and other data used to calculate the collision integrals for interactions between pairs of neutral species, between neutral species and ions, between neutral species and electrons, and between pairs of charged species.

Neutral–Neutral Interactions

Many types of intermolecular potential have been used to determine the collision integrals for interactions between neutral species. For example, Aubreton and coauthors performed calculations of Hulbert–Hirschfelder and exponential repulsive potentials, whose parameters were evaluated by non-linear regression to known potential energy curves of electronic bounded and unbounded states, respectively, for a wide range of species [2, 16, 17]. Besides the accuracy of original potential energy curves, the uncertainty of such approach mainly arises from the accuracy of the fit. For a good fit, the energy values must be reproduced as accurately as possible by the potential function. However, under some conditions, it is debatable whether the fitted potential is accurate outside the fitting range. André et al. [18] used the classical Lennard–Jones potential and simple combining rules for the potential parameters of neutral–neutral interactions to obtain the transport coefficients for nitrogen and hydrogen plasmas, and plasmas of composition corresponding to the Mars and Titan atmospheres, obtaining satisfactory agreement with the results of other authors who used more complex approaches.

To evaluate the collision integrals for the H_2O–H_2O interaction, two analytic expressions, the Stockmayer and exponential repulsive potential, were applied to the low and high temperature ranges respectively, with cubic spline functions being used to connect the collision integral values smoothly (with continuous first and second derivatives) at the intermediate temperature. This approach is based on the facts that the exponential potential only describes accurately the high energy repulsive wall of the interaction, whereas the parameters of Stockmayer potential are generally adjusted to fit the low energy attractive region of the interaction. The parameters used to determine these potential forms are obtained from a reevaluation of the stable molecule [19]; the approach provides reliable data for the collision integrals.

Recently, a new phenomenological model potential developed by Capitelli et al. [20], [21] has been widely studied. The phenomenological potential provides an improved representation of the short-range region with a less hard repulsive wall, and moreover reproduces very well the interaction obtained by accurate ab initio calculation in the long-range region. When comparing with complete set of quantum mechanical interaction potentials arising from the electronic configurations of separate partners, excellent agreement is achieved [22]. Therefore, it can provide an accurate estimation of those interaction potentials for which reliable experimental data or accurate theoretical calculations are not available. Recently, this classical model potential, which as an improvement of the Lennard–Jones potential, has been used in determining the transport coefficients of plasmas of composition corresponding to the Mars atmosphere [23, 24].

The phenomenological potential has the following form

$$\varphi = \varepsilon_0 \left[\frac{m}{n(x) - m} \left(\frac{1}{x} \right)^{n(x)} - \frac{n(x)}{n(x) - m} \left(\frac{1}{x} \right)^{m} \right] \tag{3}$$

where $x = r/r_e$, $n(x) = \beta + 4\chi^2$ and the parameter r_e is the equilibrium distance. β is determined by a simple empirical formula with the polarizability α as the input parameter.

$$\beta = 6 + \frac{5}{s1 + s2} \tag{4}$$

where the subscripts 1 and 2 identify the colliding partners. The softness s, entering in Eq. (4), is defined as the cubic root of the polarizability.

Unfortunately, experimental data are extremely limited for polarizabilities of most species that are present in our work. Coverage of dipole polarizabilities is particularly sparse. However, for these species, quantum chemical predictions for polarizabilities can be quite accurate if determined with a good correlated method. In Table 1, we present the polarizability values and their data sources.

We developed a new computer program, based on the work of Barker, Fock and Smith [35], to compute the collision integrals for the phenomenological potential.

Neutral–Ion Interactions

For neutral–ion Interactions, two kinds of processes should be taken into account, purely elastic collisions and the resonant charge-exchange inelastic process. For l odd ($l = 1$ and 3), the latter plays important role in determining the collision integrals $\Omega_{ij}^{(l,s)}$. We follow the work of Murphy [36] and estimate the total collision integrals from the elastic and inelastic contributions with the empirical mixing rule:

$$\Omega^{(l,s)} = \sqrt{\left(\Omega_{in}^{(l,s)}\right)^2 + \left(\Omega_{el}^{(l,s)}\right)^2} \tag{5}$$

where the subscripts in and el denote the collision integrals derived from the inelastic and the elastic interactions, respectively.

The phenomenological potential model has been extended to neutral–ion elastic interactions [20, 21]. The polarizability values needed for ion species and the sources of these data are tabulated in Table 2; only the ground states of the ions were considered. For the species denoted by [*] in Table 2, Woon's quantum chemical values of the polarizabilities, predicted by means of the finite field approach, were used.

Table 1 Polarizability values of neutral species (Å^3)

Species	Polarizability	Data source	Species	Polarizability	Data source
C	1.760	[25]	C_2	5.074	[26]
C_3	5.179	[26]	C_4	7.512	[26]
C_5	11.164	[26]	H	0.668	[25]
H_2	0.810	[25]	O	0.802	[25]
O_2	1.562	[27]	O_3	3.210	[28]
CH	1.394	[26]	CH_2	2.120	[26]
CH_3	2.335	[26]	CH_4	2.448	[27]
C_2H	4.415	[26]	C_2H_2	3.487	[27]
C_3H	5.539	[26]	C_4H	7.151	[26]
C_5H	10.504	[26]	C_6H	13.679	[26]
C_2H_4	4.009	[25]	C_3O_2	6.873	[33]
CO	1.951	[25]	CO_2	2.597	[29]
C_2O	4.087	[26]	OH	1.070	[30]
H_2O	1.429	[31]	HO_2	1.954	[26]
H_2O_2	2.243	[26]	CHO	2.538	[26]
CH_2O	2.450	[27]	CH_3O	2.900	[26]
CH_3OH	3.081	[27]	CH_2OH	3.000	[26]
C_2H_4O	4.560	[32]	HCOOH	3.319	[26]
C_2H_6O	5.110	[26]	COOH	3.318	[34]

Table 2 Polarizability values of charged species (Å^3)

Species	Polarizability	Data source	Species	Polarizability	Data source
C^+	0.829	[37]	C^{++}	0.578	[38]
C^{+++}	0.289	[23]	C^-	7.280	[*]
C_2^-	3.660	[*]	C_2^+	3.200	[*]
H^-	27.0	[39]	H_2^+	0.424	[40]
H_3^+	0.463	[41]	O_2^-	1.581	[34]
O_2^+	0.958	[34]	O^+	0.376	[37]
O^{++}	0.228	[23]	O^{+++}	0.182	[23]
O^-	3.200	[42]	CH^+	1.1299	[*]
CO^+	1.341	[34]	CO_2^+	2.212	[34]
CO_2^-	7.765	[34]	OH^-	6.956	[42]
H_3O^+	0.964	[43]	CHO^+	1.341	[44]
HCO_3^-	5.100	[45]	CO^-	14.153	[34]
H_2^-	31.782	[34]	OH^+	0.591	[34]
HO_2^-	3.351	[34]	H_2O^+	0.792	[34]
CH^-	7.331	[34]			

For the H^+–H, H^+–O and H^+–C interactions, previous studies of collision integrals with complete set of quantum mechanical interaction potentials arising from the electronic configurations of separate partners have been used here since the polarizability of the species H^+ was not available. For H^+–H interaction, accurate potential energy curves are available for

the two electronic terms $^2\Sigma_g$ and $^2\Sigma_u$ of the H_2^+ system and have been fitted with the Hulburt–Hirschfelder and modified Morse potential respectively [46]. For H^+–O and H^+–C interactions, the Hulburt–Hirschfelder and exponential repulsive potential were used to represent the bounded states and unbounded states respectively using nonlinear regression [16].

No accurate experimental data or theoretical calculations are available in the literature for the polarizability of HO_2^+. Hence, collision integrals for interactions involving the species HO_2^+, as well as the interaction between H^+ and other neutral species, have been derived using a polarization potential model:

$$\varphi_{in}(r) = \left(\frac{1}{4\pi\varepsilon_0}\right)^2 \frac{(Z_i e)^2 \alpha_n}{2r^4} \tag{6}$$

z_i being the ion charge and α_i being the polarizability of the neutral species. Note that the polarization potential, unlike the phenenomelogical potential, is independent of the polarizability of the charged species.

The collision integrals for the polarization potential were obtained by a closed form, which leads to simple relations as follows [46]

$$\Omega_{i,n}^{(1,1)} = 424.443 Z_i \frac{\sqrt{\alpha_n}}{T}$$

$$\Omega_{i,n}^{(1,2)} = 0.833\Omega_{i,n}^{(1,1)} \quad \Omega_{i,n}^{(2,2)} = 0.870\Omega_{i,n}^{(1,1)} \quad \Omega_{i,n}^{(1,3)} = 0.729\Omega_{i,n}^{(1,1)} \quad \Omega_{i,n}^{(2,3)} = 0.761\Omega_{i,n}^{(1,1)}$$

$$\Omega_{i,n}^{(1,4)} = 0.656\Omega_{i,n}^{(1,1)} \quad \Omega_{i,n}^{(2,4)} = 0.685\Omega_{i,n}^{(1,1)} \quad \Omega_{i,n}^{(1,5)} = 0.602\Omega_{i,n}^{(1,1)} \quad \Omega_{i,n}^{(3,3)} = 0.842\Omega_{i,n}^{(1,1)} \tag{7}$$

In order to numerically evaluate the charge transfer collision integrals, it is necessary to know the charge transfer cross section. For interactions between a parent atom or molecule X and its ion X^- or X^+, especially for high energies, the transport cross section can be evaluated by from charge transfer cross-section written as

$$Q^l(g) = 2Q_{ex} \tag{8}$$

The charge transfer cross section is approximated by the following representation:

$$Q_{ex} = (A - B\ln E)^2 \tag{9}$$

where E is the collision energy. The constants A and B can be obtained from experiment data or theoretical calculations. The charge exchange cross-sections for collisions between unlike species (e.g. $Y^\pm + X \rightarrow X^\pm + Y$) are small compared to the elastic collision integrals, and are neglected in this paper. Collision integrals with even l are wholly determined by the elastic interactions.

In Table 3, we present the constants A and B that characterize the resonant charge exchange cross-sections considered in this work.

No accurate experimental data or theoretical calculations are available in the literature for the charge-exchange interactions between C and C^-. The constants A and B were determined using an empirical formula proposed in Ref. [53].

Electron–Neutral Interactions

The collision integrals for interactions between electrons and neutral species have been calculated as a function of temperature by straightforward integration of the $Q_1(E), Q_2(E)$

Table 3 Constants A and B hat characterize resonant charge exchange

Interaction	A	B	Data source
$H–H^+$	6.6989	0.3874	[47]
$H_2–H_2^+$	4.8082	0.4082	[48]
$H–H^-$	13.6059	1.2734	[49]
$C–C^+$	8.4908	0.4383	[50]
$O_2–O_2^+$	6.8007	0.3976	[48]
$O_2–O_2^-$	4.8632	0.2703	[51]
$O–O^-$	9.5408	0.6387	[52]
$CO–CO^-$	8.3415	0.3780	[48]
$CH–CH^+$	9.2119	0.4324	[48]
$OH–OH^-$	12.1052	0.8435	[48]
$OH–OH^+$	7.6751	0.3986	[48]
O–O	6.1152	0.2859	[52]

and $Q_3(E)$ cross-sections as a function of electron energy, assuming a Boltzmann distribution. When $Q_2(E)$ and $Q_3(E)$ are not available, their ratios to the momentum transfer cross section $Q_1(E)$can be determined by numerical integration of differential elastic cross sections (DCS), if these are available. The differential cross sections $d\sigma/d\Omega$ can be numerically integrated over all scattering angles to obtain the transport cross sections as a function of the interaction energy.

For e–H_2 interaction, following the recommendation of Brunger and Buckman [54], the momentum transfer cross-section evaluated by England et al. [55] was used in this work. The corrections to higher momentum transport cross-sections, $Q^2(E)/Q^1(E)$ and $Q^3(E)/Q^1(E)$, have been obtained by integrating the elastic differential cross sections given in Refs. [56, 57].

For the e–H interaction, the momentum transfer cross-section recommended by Itikawa was used [58]. The transport cross-section ratios $Q^2(E)/Q^1(E)$ and $Q^3(E)/Q^1(E)$ were revaluated by integrating the elastic differential cross sections from [59] and [60] and extrapolated down to an energy of 0.01 eV using the limiting value at zero energy, i.e. 2/3 for $Q^2(E)/Q^1(E)$ and 1 for $Q^3(E)/Q^1(E)$.

The momentum transfer cross sections evaluated by Itikawa (0.01–100 eV) were used for the e–O_2 interaction [61]. The momentum transport cross-section ratios $Q^2(E)/Q^1(E)$ and $Q^3(E)/Q^1(E)$ were obtained using the elastic differential cross sections presented in Refs. [62–64]. For the energy range above 100 eV, the transport cross sections were obtained by direct numerical integration of the elastic differential cross sections in [64].

The e–O collision cross sections were determined using the experimental elastic differential cross-sections of Williams (0.54, 2.18, 3.4, 4.9, 8.71 eV) [65], supplemented by those of Thomas at 11 eV [66] and Blahain in the energy range (15 eV to about 500 eV) [67]. In the lower energy range, the momentum transport cross-section ratios $Q^2(E)/Q^1(E)$ and$Q^3(E)/Q^1(E)$ were estimated from the recommended momentum transport cross sections of Itikawa [68], together with the limiting values of the ratios.

The e–OH interaction collision integrals were calculated from the same data source as was used in Ref. [17]. For electron energies from 2 to 500 eV, the theoretical differential cross-sections of Sobrinho et al. [69], supplemented by those of Chen et al. [70] for $E = 1.58$ eV, were used to determine the transfer cross sections by numerical integration. In lower energy range to 0.01 eV, a similar extrapolation technique was adopted to that mentioned above.

For the e–H_2O interaction, differential cross sections measured at incident energies of 1, 2, 4, 6, 8, 10, 15, 20, 30, 50 and 100 eV [71], supplemented by data at 0.25 eV [72] and 200 and 500 eV [73], were used to obtain the transport cross sections. For the lower energy range to 0.01 eV, the momentum transfer cross-sections recommended in Ref. [74] were used to extrapolate the other data, using the above-mentioned method.

As regards the e–CO_2 collision, measured differential cross sections for low- and intermediate-energy (1–50 eV) elastic electron scattering from CO_2 [75] and theoretical data in the energy range (50–500 eV) [76] were used to numerically determine the transport cross sections. These data were supplemented at lower energies with the recommended momentum transport cross-section of Itikawa [77].

For the e–CO interaction, differential cross-section data in the energy range 1–30 eV were taken from Gibson et al. [78], supplemented by the data of Allan in the energy range 0.2–5 eV [79]. The elastic collision differential cross sections in higher energy between $30 \sim 500$ eV were taken from theoretical studies [80]. These data were supplemented at lower energies by the integral momentum transfer cross-sections based on swarm experiments from Land [81].

For the high energy e–CH_4 interaction (from 5 to 200 eV), the theoretical data of Lee et al. [82] and the experimental results of Cho et al. [83] were used. For intermediate energies (from 0.1 to 5 eV), the differential cross sections of Bundschu et al. [84] were used (for six values of electron energy from 0.6 to 5 eV) and were complemented by those of Sohn et al. [85]. For the lower energy range (from 0.01 to 0.1 eV), the momentum transfer cross-section obtained by Cho et al. [83] was used to evaluate the other data using the above-mentioned extrapolation technique.

The momentum transfer cross sections for the e–C_2H_2 interaction were derived from the electron swarm parameters measured by Nakamura [86]. These values have good agreement with other studies [87, 88]. The transport cross-section ratios $Q^2(E)/Q^1(E)$ and $Q^3(E)/Q^1(E)$ were determined by the numerical integration of the differential cross-section data from these studies, supplemented by the theoretical calculation in higher energy range (above 100 eV) given in Ref. [89].

A theoretical study on elastic e–CH_x ($x = 1, 2, 3$) collisions in the energy range from 0.1 to 500 eV presented in Refs. [90, 91] was used to determine the transport cross-sections. For the energies below 0.1 eV, extrapolation of the momentum transfer cross-section to 0.01 eV was carried out using polynomials fitted to the nearest few points, taking the original shapes as a reference.

For elastic e–C_2O collisions, theoretical data, including momentum and differential transport cross-sections, in the energy range from 1 to 500 eV given in Refs. [92, 94] were utilized to obtain the transport cross-sections. Similar methods to those mentioned above were used to extrapolate the data to 0.01 eV.

Average cross sections given previously in Refs. [7, 23, 93] were used for the e–C, e–C_2, e–C_3 and e–O_3 interactions. For other electron–neutral interactions, unfortunately, to our knowledge, no available experimental or calculated data are available in the literature. The cross-sections were estimated by assuming that the cross-sections are independent of energy and dominated by polarization effects [95]. These crude approximations mean that the values of electrical conductivity at low levels of ionization are not likely to be accurate [96]. However, these uncertainties are not important for the condition considered here for two reasons. First, because electron–ion collision cross-sections are about three orders of magnitude greater than electron–neutral cross-sections, accurate values of the latter cross-sections are important only for small degrees of ionization (<1 %). Second, when

ionization begins, the concentrations of those species for which these estimates were adopted are extremely low, so the effect on the electrical conductivity is negligible.

Charged–Charged Interactions

These interactions were described by a Coulomb potential screened at the shielding distance of the Debye length by the presence of charged particles. The effective collision integrals were calculated from the works of Mason et al. [97], [98], in which the Debye length is calculated taking into account only electrons. This is a standard procedure that leads to a larger value of the Coulomb collision integrals. In fact, as to whether the heavy particles should be taken into account in the Debye shielding effect, there is large conflict. From previous study, it would give better agreement with experimental results under the condition that calculations are made using the screened Coulomb potential if ions were not considered in the Debye radius. For these reasons, electrons only are considered in calculating the Debye radius [99].

Results and Comparisons

Application to H_2O and CO_2 Plasmas

The equilibrium properties of pure water and carbon dioxide plasmas have been studied in the literature, due to their importance for many applications. There are few experimental measurements of transport coefficients at high temperatures, so it is important to check the consistency of our equilibrium calculations with other results. Our results compare generally satisfactorily with most of theoretical results presented by different authors as can be seen in Figs. 1 and 2, which display viscosity and thermal conductivity data.

For the viscosity of pure water vapour, excellent agreement is found with the results of Aubreton et al. [17], except for a slight discrepancy in the low temperature range for which dissociation does not occur; this deviation is attributable to the use of a different potential for the H_2O–H_2O interaction. Large deviations from Krěnek's results are apparent; these occur because of the different collision integrals used, especially in the temperature range in which chemical reactions occur. Two classic potentials (Lennard–Jones 6–12 and polarizability potentials) were used by Krěnek in his work [101]. Recent studies comparing these potentials (which have the advantage of being easily calculated) with those obtained from accurate ab initio calculations have emphasized that estimates of the interaction energy from the two classic potentials can be poor, and often lead to large errors [98].

Our calculated viscosity of CO_2 closely follows the results by André et al. [18] closely reproducing the peak value. It has been demonstrated for several ion–neutral interactions that the ratio of the viscosity and diffusion collision integrals is underestimated when the polarization potential is used [7, 100]. The slightly higher value by André et al. can be explained by this. The agreement is generally acceptable when compared with the calculations of Aubreton et al. [2], the differences arising from the accuracy of evaluation of the relevant interactions, in particular $C–O^+$ and $O–C^+$. In Aubreton et al.'s work, not all the electronic states were taken into account in the statistical computation of the collision integrals, due to the unavailability of the required data. In contrast, large differences between our results and those of other authors can be found; our results should be more reliable because of the good performance of the phenomenological potential in describing the average interaction potential. Additionally, there is no influence on the properties of

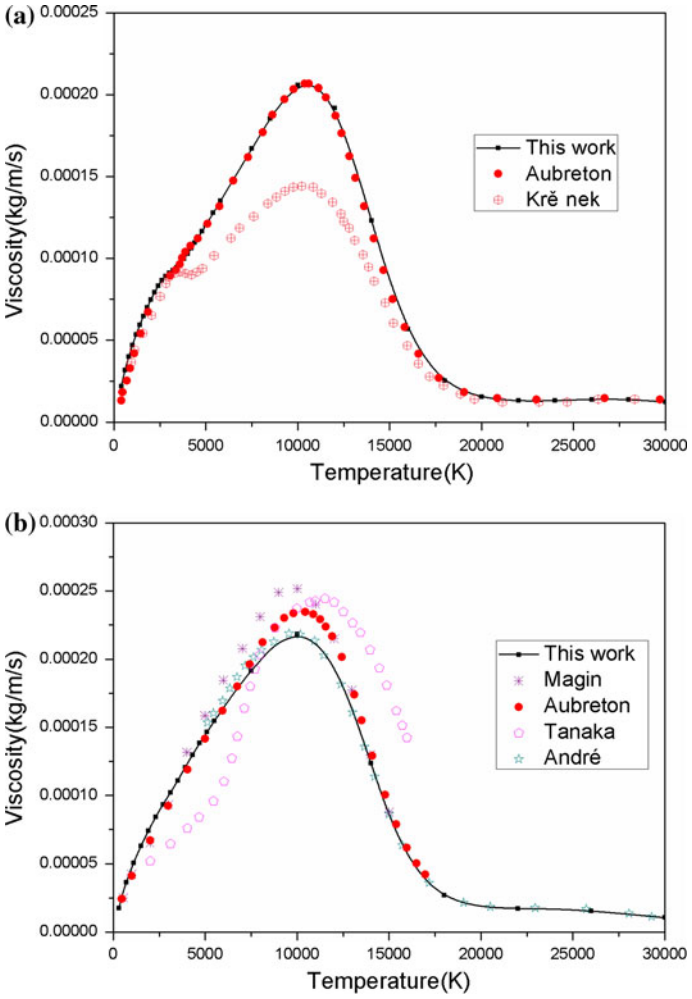

Fig. 1 Temperature dependence of viscosity of H_2O and CO_2 at atmospheric pressure. The calculated results of Krěnek [101] and Aubreton et al. [17] for H_2O, and Magin et al. [102], André et al. [18], Tanaka et al. [3] and Aubreton et al. [2] for CO_2, are shown for comparison

CO_2 plasmas whether solid carbon is taken into account or not in the computation due to its extremely small amount.

We have plotted the thermal conductivity of pure water vapour and carbon dioxide plasmas in Fig. 2. As in the case of viscosity, our calculated thermal conductivity for pure water agrees well with the results of Aubreton et al. [17] and large deviations from the results of Krěnek [101] occur. General agreement was found with the work of André et al. [18] and Aubreton et al. [2] for CO_2. The difference occurs mainly in the temperature range in which the ionization reactions occur. Our elastic collision integrals for $O–O^+$, determined using the phenomenological potential, are in close agreement with those obtained by the accurate ab initio calculation, and the charge-exchange collision integrals also agree quite well. The difference in the height of the third peak arises partly from the large discrepancy of the charge-exchange cross section for the $C–C^+$ interaction, and partly from

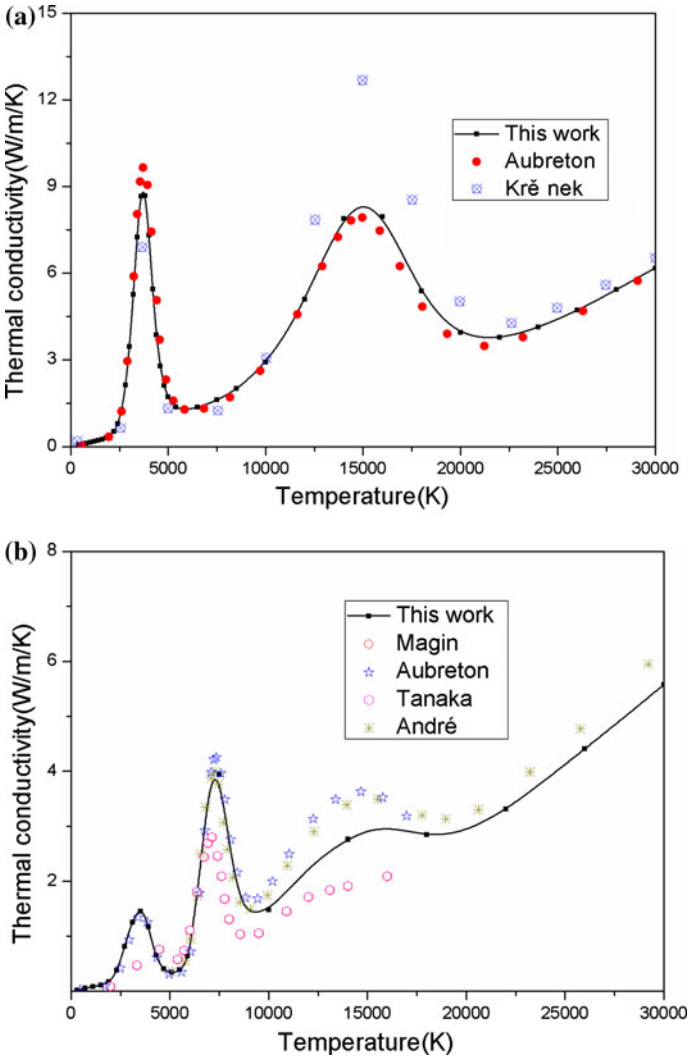

Fig. 2 Temperature dependence of thermal conductivity of H_2O and CO_2 at atmospheric pressure. The calculated results of Křenek [101] and Aubreton et al. [17] for H_2O, and Magin et al. [102] and André et al. [18], Tanaka et al. [3] and Aubreton et al. [2] for CO_2, are shown for comparison

the different definitions of the Debye length. The Debye length plays an important role in determining the collision integrals between charged species. In the present work, only the shielding effect of electrons is taken into account, which leads to larger values of the Coulomb collision integrals. In André et al.'s work, the contributions from both the electrons and ions were considered.

Equilibrium Transport Coefficients for $C_q(H_2O)_{1-q}$ Mixtures

Figures 3, 4, 5, 6 and 8, respectively show the electron thermal diffusion coefficients, viscosity, thermal conductivity and electrical conductivity of the mixture $C_q(H_2O)_{1-q}$

calculated in the temperature region 400–30,000 K and at atmospheric pressure. The molar amount of water varies from 0 (pure water vapour) to 1 (pure carbon) in steps of 0.1. Figure 7 shows the components of the thermal conductivity for $q = 0.8$.

$C_q(H_2O)_{1-q}$ mixtures have almost identical electron thermal diffusion coefficients values between 16,000 and 20,000 K, because interactions between electrons and singly-ionized ions dominate. Above 20,000 K, the addition of carbon to water decreases the

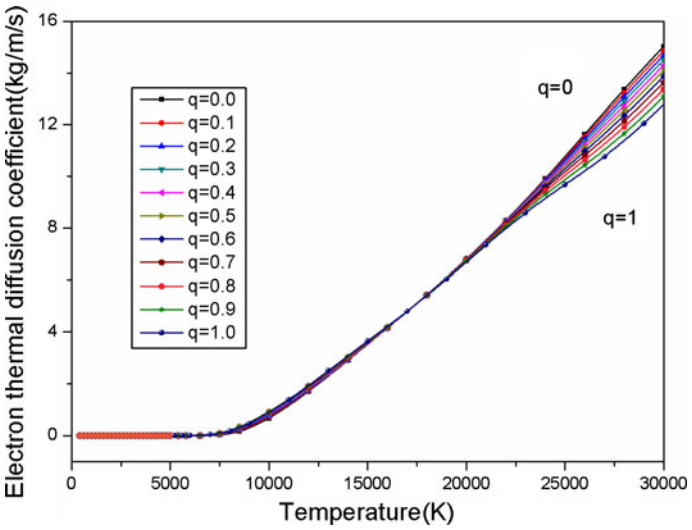

Fig. 3 Temperature dependence of electron thermal diffusion coefficients of carbon and water mixtures for molar amounts of carbon q from 0 to 1 in steps of 0.1 at atmospheric pressure

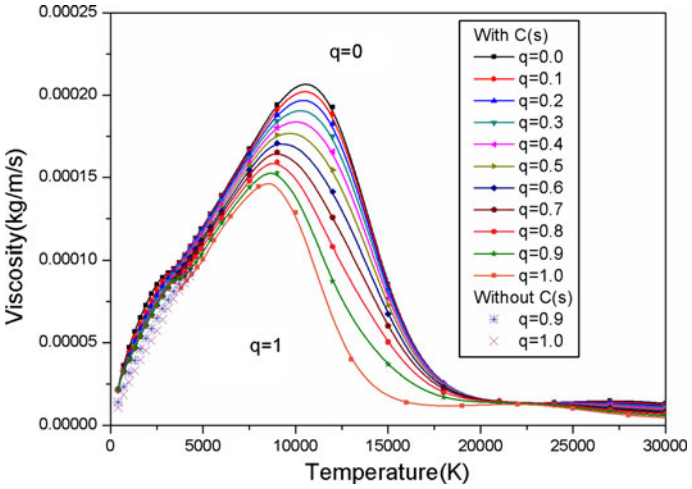

Fig. 4 Temperature dependence of viscosity of carbon and water mixtures for molar amounts of carbon q from 0 to 1 in steps of 0.1 at atmospheric pressure considering (*solid and symbol lines*) and neglecting (*symbols* for $q = 0.9$ and 1) condensed carbon

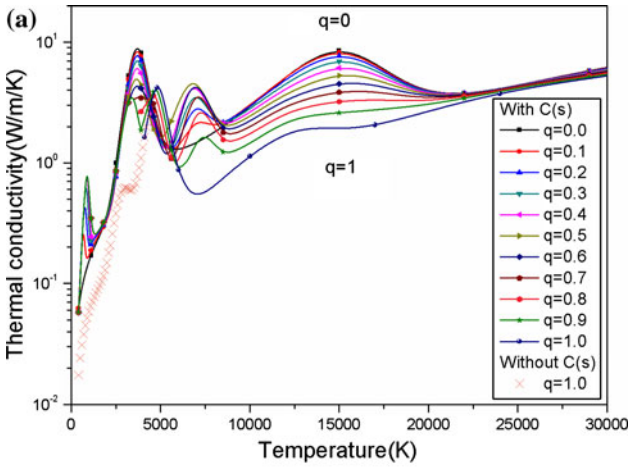
(a)
q=0
q=1
With C(s)
q=0.0
q=0.1
q=0.2
q=0.3
q=0.4
q=0.5
q=0.6
q=0.7
q=0.8
q=0.9
q=1.0
Without C(s)
q=1.0
Thermal conductivity(W/m/K)
Temperature(K)

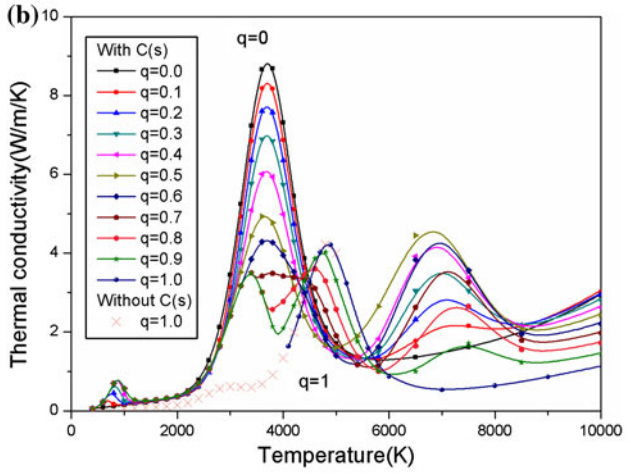
(b)
q=0
q=1
With C(s)
q=0.0
q=0.1
q=0.2
q=0.3
q=0.4
q=0.5
q=0.6
q=0.7
q=0.8
q=0.9
q=1.0
Without C(s)
q=1.0
Thermal conductivity(W/m/K)
Temperature(K)

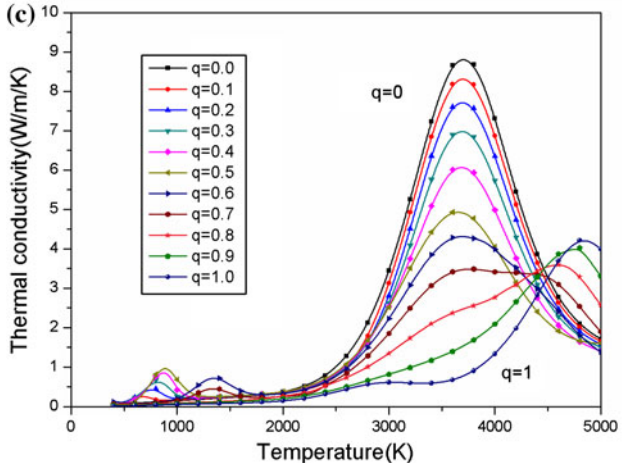
(c)
q=0
q=1
q=0.0
q=0.1
q=0.2
q=0.3
q=0.4
q=0.5
q=0.6
q=0.7
q=0.8
q=0.9
q=1.0
Thermal conductivity(W/m/K)
Temperature(K)

◀ **Fig. 5** Temperature dependence of thermal conductivity of carbon and water mixtures for molar amounts of carbon q from 0 to 1 in steps of 0.1 at atmospheric pressure considering (**a**, **b**) and neglecting (**c**) condensed carbon. **a** Logarithmic scale. **b** Detail of low-temperature range of Fig. 5a, linear scale. For pure carbon, the case without considering solid carbon is also presented for comparison in Figs. 5a, b (*symbols*)

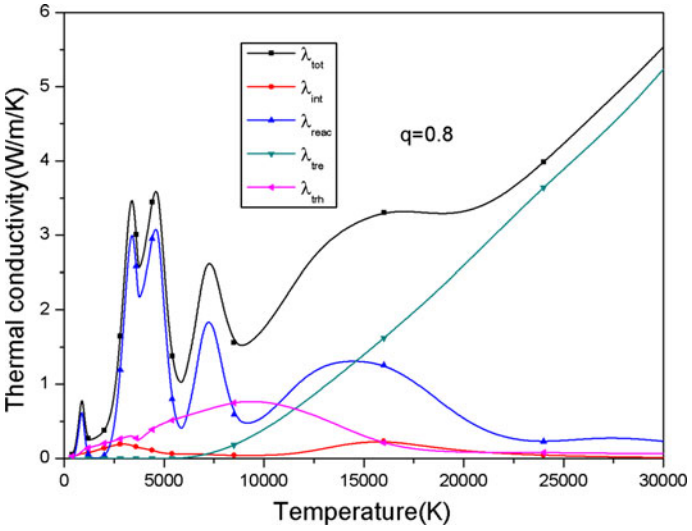

Fig. 6 Temperature dependence of the components of thermal conductivity of the carbon and water mixture with molar amount of carbon $q = 0.8$ at atmospheric pressure, with solid carbon included

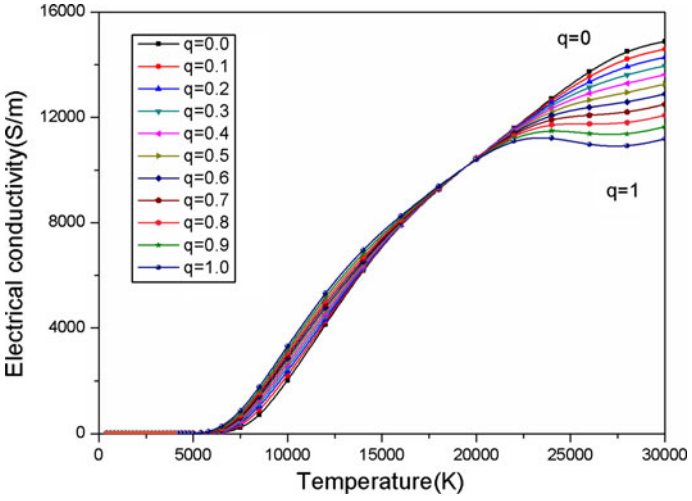

Fig. 7 Temperature dependence of electrical conductivity of carbon and water mixtures for molar amounts of carbon q from 0 to 1 in steps of 0.1 at atmospheric pressure

electron thermal diffusion coefficients, as can seen in Fig. 3. Solid carbon, which is present only below the ionization temperature, has negligible influence on the electron thermal diffusion coefficients, so the corresponding results are not presented here.

The viscosity is a measure of momentum transport, which establishes the proportionality between the frictional force in the direction of the flow and the velocity gradient in the orthogonal direction. For pure gas, as a first approximation, viscosity is proportional to the square root of the product of mass and temperature and inversely proportional to the collision integrals, particularly for charged species mole fractions below 1 %. The change in the slope at 3,500 K for pure water is due to the dissociation of diatomic hydrogen and oxygen molecules, which leads to changes of collision integrals (from intermolecular interactions to interatomic interactions) and a halving of the particle mass. At higher temperatures the differences are much smaller because the mixture is already nearly fully ionized and interactions of charged particles prevail. At these temperatures, the viscosity decreases as a result of the large collision integrals for the Coulomb interaction between charged particles. The addition of carbon to water increases the viscosity of the mixture and shifts its peak position, which occurs in the temperature range in which the atoms ionize, to higher temperature. This shift can be explained by the lower ionization temperature of carbon atoms, compared to those of oxygen and hydrogen atoms. Mixtures of carbon and water generally show viscosity values intermediate to those of the pure gases.

The influence of solid carbon on the viscosity can be seen in Fig. 4. Below the sublimation temperature, the values of viscosity for different mixing ratios are almost identical, so only results for $q = 0.9$ are shown. This is because if the solid phase appears at a given temperature, the mole fractions of the main gaseous species will not change even if more carbon is added to the reaction system because the system has arrived at a dynamic equilibrium. Of course, viscosities for pure carbon ($q = 1$) differ from those of the mixtures because different gas phase species are present. By comparing the viscosities obtained with and without taking account of the solid carbon for the case of $q = 0.9$ shown in Fig. 4, we can see that neglecting solid carbon increases the viscosity.

We have plotted the thermal conductivity of carbon and water mixtures at atmospheric pressure in Fig. 5. In most situations, the thermal conductivity of carbon and water mixtures has values intermediate to those of the pure gases. However, an "anomalous" behaviour, which is a departure from this tendency, exists in our results. These phenomena occur mainly in the temperature ranges 4,200–12,500 K regardless of the inclusion of solid carbon together with the temperature range below 2,000 K if solid carbon is neglected in the computation.

If the phase transition is taken into account, there are four peaks for C/H_2O ratio $q \leq 0.5$, which correspond respectively to the successive dissociations of the polyatomic species CH_4, H_2O and CO_2 into H_2 and CO, the dissociation of CO, the dissociation of H_2, and the first ionization of C, H and O atoms. For $q > 0.7$, one more peak related to the dissociation of carbon molecules and hydrocarbon radicals appears. For $q = 0.7$, the peaks associated with the dissociation of hydrogen molecules and hydrocarbon radicals are superimposed and are not easy to distinguish. With the addition of carbon, the amplitude of the peak related to the dissociation of molecular hydrogen decreases due to the reduction of the total hydrogen mole fraction. In contrast, the peak value corresponding to the dissociation of molecular carbon and hydrocarbon radicals increases.

If solid carbon is not taken into account, the thermal conductivity changes significantly for some cases as depicted in Fig. 5c. For $q = 0.1$ and 0.2, no solid carbon appears in the system, so the thermal conductivity is unchanged. For $q = 0.3$, 0.4 and 0.5, the first peak in the thermal conductivity, which is caused by the dissociation of the polyatomic species CH_4, H_2O and CO_2 into H_2 and CO, increases in magnitude compared to its values when solid carbon is included. For $q = 0.6$ and 0.7, the first peak is shifted to higher temperature and is decreased in magnitude. For $q = 0.8$ and 0.9, the amount of molecular hydrogen is greatly reduced due to the small water fraction, and no obvious peak that corresponds to its

decomposition occurs. For pure carbon, the first two peaks are associated with the successive dissociation of carbon molecules. Taking $q = 0.5$ as an boundary, when $q \leq 0.5$, CH_4 and CO_2 mainly dissociate into CO and H_2 in the temperature of around 900 K and with increasing value of q, the maximum mole fraction of CH_4 appearing in the system increases and hence the height of the first thermal conductivity peak increase; when $q > 0.5$, as carbon is further added into the mixture, large amount of CO appears and CH_4 mainly dissociates into H_2 and hydrocarbons such as C_2H_2 in a higher temperature of around 1,300 K. With increasing value of q, the maximum mole fraction of CH_4 and hence the height of the first thermal conductivity peak decrease.

The thermal conductivity is the sum of four components: the heavy-particle translation thermal conductivity, the electron translation thermal conductivity, the internal thermal conductivity and the reaction thermal conductivity. These components are shown for $q = 0.8$, with solid carbon taken into account and for atmospheric pressure, in Fig. 6. The reaction conductivity contributes strongly to the form of the total thermal conductivity, and the electron translational component is the dominant term for temperature above 20,000 K. The influence of solid carbon, which suddenly disappears at the phase transition temperature, leads to a rapid increase and discontinuity in some components.

The electrical conductivity is directly related to the electron density, i.e. the ionization degree of the plasma. Below temperatures around 18,000 K, the ionization temperature decreases as the carbon proportion increases, due to the lower ionization energy of carbon atoms relative to those of hydrogen and oxygen atoms, and hence the electrical conductivity increases. Above 22,000 K, as the mole fraction of carbon increases, the electrical conductivity of the mixture decreases even though the electron number density rises (see Ref. [1]). This can be explained by referring to the first approximation expression of electrical conductivity:

$$\sigma(1) = \frac{3e^2 n_e}{8\sqrt{2\pi kTm_e}\sum_{j\neq e}^{v} n_j \overline{\Omega}_{e,j}^{(1,1)}} \tag{10}$$

As more carbon is added to the water vapour, the increasing electron number density is counteracted by the influence of the formation of multiply-charged ions, for which the Coulomb collision integrals are larger. Because carbon ion has lower second ionization energy, C^{2+} ions are formed at a lower temperature than O^{2+} and H^{2+} ions. The decrease of the electrical conductivity as temperature increases in this temperature range is also a consequence of multiple ionization.

Including the carbon phase transition has negligible influence on the electrical conductivity, since significant ionization does not occur at the relevant temperatures.

Influence of Pressure on Transport Properties

Taking the case of $q = 0.8$ as an example, the influence of pressure on the transport coefficients is illustrated in Figs. 8, 9, 10, 11. According to Le Chatelier's principle, an increase of the pressure opposes changes to the original state of equilibrium, so that dissociation and ionization at a given temperature are suppressed. Therefore, the peaks of the specific heat at constant pressure, viscosity, thermal conductivity are shifted to higher temperature, as was the case of the specific heat at constant pressure discussed in the first paper of this series [1].

The maximum value of the viscosity increases with pressure. This is because of the suppression of ionization, which means that the strong Coulomb interactions do not

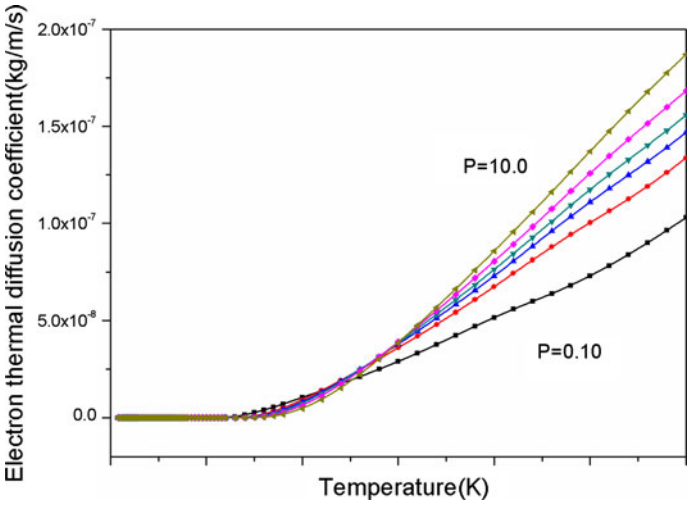

Fig. 8 Temperature dependence of the electron thermal diffusion coefficients at pressures of 0.1, 1, 2, 3, 5 and 10 atm.

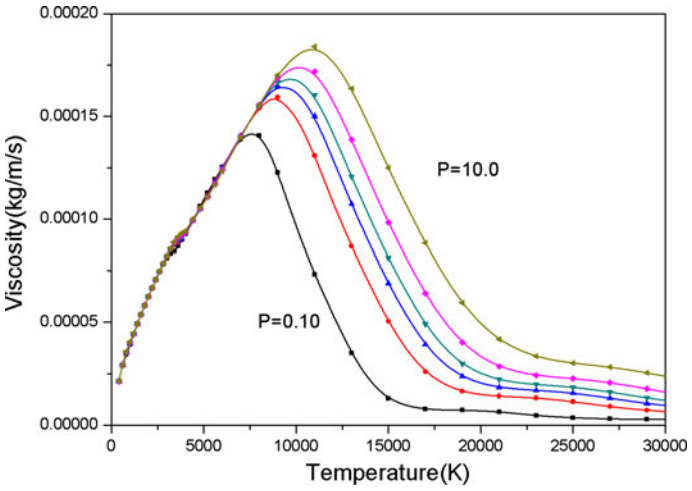

Fig. 9 Temperature dependence of the viscosity at pressures at pressures of 0.1, 1, 2, 3, 5 and 10 atm.

dominate until higher temperatures. At temperatures below that at which the viscosity maximum occurs for the lowest pressure, the influence of pressure is only small, and is due to the changes in the dissociation temperatures.

Changing the pressure changes the temperature at which the thermal conductivity peaks occur. This is again due to suppression of dissociation and ionization, which shifts the peaks in reaction thermal conductivity to higher temperature. In addition, the amplitudes of the peaks associated with the dissociation and ionization reactions are reduced and increased respectively.

The values of the electron thermal diffusion coefficients and electrical conductivity decrease as the pressure increases at temperatures below about 12,000 K, as illustrated in

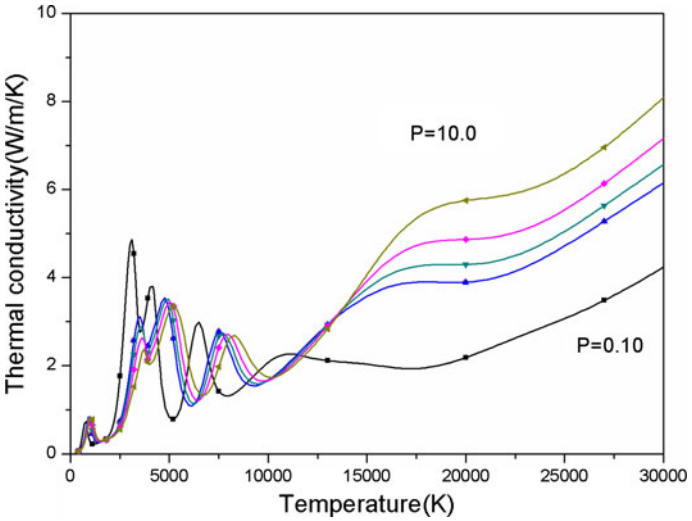

Fig. 10 Temperature dependence of the thermal conductivity at pressures of 0.1, 1, 2, 3, 5 and 10 atm.

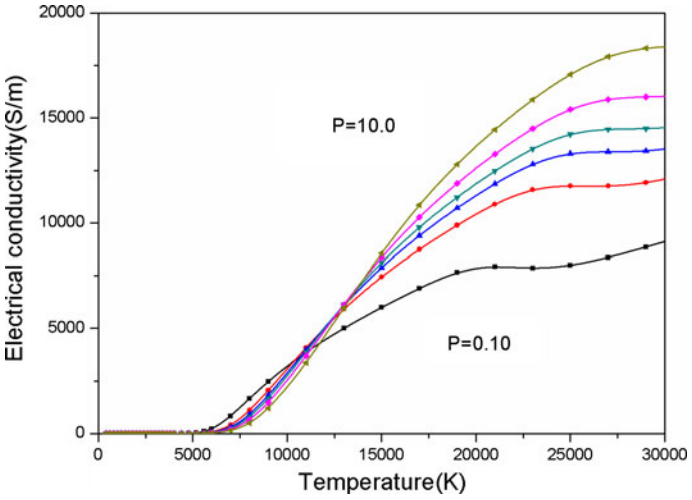

Fig. 11 Temperature dependence of electrical conductivity at pressures of 0.1, 1, 2, 3, 5 and 10 atm.

Fig. 11. This is because the ionization temperature increases with pressure, so the ionization degree is lower at a given temperature. Above about 12,000 K, the electron number density (described in Fig. 12), and thus both the electron thermal diffusion coefficients and the electrical conductivity, increase with pressure.

Discussion and Conclusion

In this paper, a considerable effort has been devoted to the calculation of transport coefficients of carbon and water plasmas in local thermodynamic equilibrium for temperatures

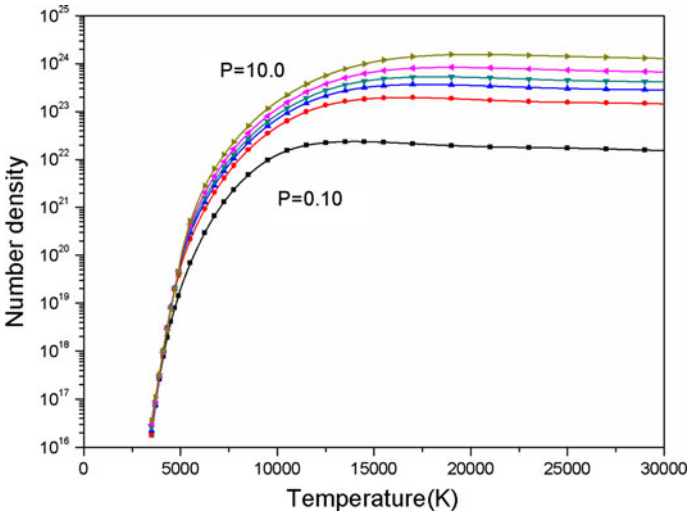

Fig. 12 Temperature dependence of electron number density at pressures of 0.1, 1, 2, 3, 5 and 10 atm.

from 400 to 30,000 K and pressures from 0.1 to 10 atm, which are conditions relevant to a wide range of applications. Use was made of collision integrals obtained by recent intermolecular interaction studies. A reliable database of high-order collision integrals involving all important neutral–neutral, neutral–ion, electron–neutral and charged–charged interactions was developed. Validation of the transport coefficients determined using these collision integrals was carried out by comparing with available data for high-temperature pure water and carbon dioxide in the literature. Generally good agreement was found with most data for pure water, particular the more recent data. Some discrepancies exist between the transport coefficients obtained here for carbon dioxide and those presented in the literature; these can be accounted for in terms of the differences between certain collision integrals used in the calculation, especially the $C–C^+$ charge transfer collision integrals. Results have been presented both taking into account and neglecting the condensed phase of carbon, and the differences have been highlighted. Our work not only fills the gap left by the lack of transport coefficient data for reacting mixtures of carbon and water, thus making possible the modelling of carbon and water plasmas, but also provides a full set of interaction collision integrals which can be applied for all other C/H/O/e mixtures. The results presented here are expected to have high accuracy, and are reliable reference data for further research on the C/H/O/e high temperature reacting system.

Acknowledgments This work was supported by the Chinese Government Scholarship program for postgraduates and the Dual Collaborative PhD Degree Program between Xi'an Jiaotong University and University of Liverpool.

References

1. Wang WZ, Murphy AB, Rong MZ, Yan JD, Spencer JW, Fang MTC (2011) Thermophysical properties of high-temperature reacting mixtures of carbon and water in the range 400–30,000 K and 0.1–10 atm. Part 1: equilibrium composition and thermodynamic properties. Plasma Chem Plasma Process. doi:10.1007/s11090-011-9327-y

2. Aubreton J, Elchinger MF, Hacala A, Michon U (2009) Transport coefficients of typical biomass equimolar CO–H_2 plasma. J Phys D Appl Phys 42:095206
3. Tanaka Y, Yamachi N, Matsumoto S, Kaneko S, Okabe S, Shibuya M (2008) Thermodynamic and transport properties of CO_2, CO_2–O_2, and CO_2–H_2 mixtures at temperatures of 300 to 30,000 K and pressures of 0.1 to 10 MPa. Electr Eng. Japan 163:18–29
4. Hirschfelder JO, Curtis CF, Bird RB (1964) Molecular theory of gases and liquids, 2nd edn. Wiley, New York
5. Chapman S, Cowling TG (1970) The mathematical theory of non-uniform gases, 3rd edn. Cambridge University Press, Cambridge
6. Ferziger JH, Kaper HG (1972) Mathematical theory of transport processes in gases. North-Holland, Amsterdam
7. Wang WZ, Rong MZ, Murphy AB, Wu Y, Spencer JW, Yan JD, Fang MTC (2011) Thermophysical properties of carbon–argon and carbon–helium plasmas. J Phys D Appl Phys 44:355207
8. Rat V, André P, Aubreton J, Elchinger MF, Fauchais P, Lefort A (2002) Transport coefficients including diffusion in a two-temperature argon plasma. J Phys D Appl Phys 35:981–991
9. Devoto RS (1973) Transport coefficients of ionized argon. Phys Fluids 16:616–623
10. Devoto RS (1967) Third approximation to the viscosity of multicomponent mixtures. Phys Fluids 10:2704–2706
11. Butler JN, Brokaw RS (1957) Thermal conductivity of gas mixtures in chemical equilibrium. J Chem Phys 26:1636–1643
12. Meador WE, Stanton LD (1965) Electrical and thermal properties of plasmas. Phys Fluids 8:1694–1703
13. Monchick L, Yun KS, Mason EA (1963) Formal kinetic theory of transport phenomena in. polyatomic gas mixtures. J Chem Phys 39:654–669
14. Hirschfelder JO (1957) Heat conductivity in polyatomic or electronically excited gases. Chem Phys 26:282–285
15. Hirschfelder JO (1957) In: Proceedings of 6th international symposium on Combustion. Reinhold, New York, p 351
16. Sourd B, Aubreton J, Elchinger MF, Labrot M, Michon U (2006) High temperatures transport coefficients in e/C/H/N/O mixture. J Phys D Appl Phys 39:1105–1119
17. Aubreton J, Elchinger MF, Vinson JM (2009) Transport coefficients in water plasma: part I: equilibrium plasma. Plasma Chem Plasma Process 29:149–171
18. André P, Aubreton J, Clain S (2010) Transport coefficients in thermal plasma. Applications to mars and titan atmospheres. Eur Phys J D 57:227–234
19. Paul P, Warnatz J (1998) In: A re-evaluation of the means used to calculate transport properties of reacting flows 27th symposium (international) on Combustion. The Combustion Institute, pp 495–504
20. Capitelli M, Cappelletti D, Colonna G, Gorse C, Laricchiuta A, Liuti G, Longo S, Pirani F (2007) On the possibility of using model potentials for collision integral calculations of interest for planetary atmospheres. Chem Phys 338:62–68
21. Laricchiuta A, Colonna G, Bruno D, Celiberto R, Gorse C, Pirani F, Capitelli M (2007) Classical transport collision integrals for a Lennard–Jones like phenomenological model potential. Chem Phys Lett 445:133–139
22. Andrea L, Federico P (2008) A comparison of interatomic potentials for rare gas nanoaggregates. J Mol Struct (Theochem) 857:22–29
23. Laricchiuta A, Bruno D, Capitelli M, Catalfamo C, Celiberto R, Colonna G, Diomede P, Giordano D, Gorse C, Longo S, Pagano D, Pirani F (2009) High temperature Mars atmosphere. Part I: transport cross section. Eur Phys J D 54:607–612
24. Catalfamo C, Bruno D, Colonna G, Laricchiuta A, Capitelli M (2009) High temperature Mars atmosphere. Part II: transport properties. Eur Phys J D 54:613–621
25. Miller TM, Bederson B (1977) Atomic and molecular polarizabilities—a review of recent advances. Adv At Mol Phys 13:1–55
26. Woon DE, Herbst E (2009) Computed dipole moments and dipole polarizabilies for neutral astromolecules. APJS 185:273–288
27. Olney TN, Cann NM, Cooper G, Brion CE (1997) Absolute scale determination for photoabsorption spectra and the calculation of molecular properties using dipole sum-rules. J Chem Phys 223:59–98
28. Lide DR (ed) (1994) CRC handbook of chemistry and physics, 7th edn. CRC, Boca Raton
29. Bose TK, Cole RH (1970) Dielectric and pressure virial coefficients of imperfect gases. II. CO_2-argon mixtures. J Chem Phys 52:140–147
30. Du S, Francisco JS, Schenter GK, Iordanov TD, Garrett BC, Dupuis M, Li J (2006) The OH radical-H_2O molecular interaction potential. J Chem Phys 124:22438

31. Cybulski SM, Haley TP (2004) New approximations for calculating dispersion coefficients. J Chem Phys 121:7711–7716
32. Applequist J, Carl JR, Fung KK (1972) An atom dipole interaction model for molecular polarizability. Application to polyatomic molecules and determination of atom polarizabilities. J Am Chem Soc 94:2952–2960
33. Stout JM, Dykstra CE (1994) Static dipole polarizabilities of organic molecules. Ab initio calculations and a predictive model. J Am Chem Soc 117:5127–5132
34. (2004) In: Johnson III RD (ed) NIST Computational Chemistry Comparison and Benchmark Database, NIST standard reference database number 101, Release 10th edn
35. Barker JA, Fock W, Smith F (1964) Calculation of gas transport properties and the Interaction of argon atoms. Phys Fluids 7:897–903
36. Murphy AB, Arundell CJ (1994) Transport coefficients of argon, nitrogen, oxygen, argon–nitrogen, and argon–oxygen plasmas. Plasma Chem Plasma Process 14:451–490
37. Thakkar A, Das AK (2001) Anisotropic polarizabilities and hyperpolarizabilities of second-period cations. J Mol Str (Theochem) 547:233
38. Shevelko VP, Vinogradov AV (1979) Static dipole polarizability of atoms and ions in the Thomas-Fermi Model. Phys Scr 19:275–282
39. Alagia M, Brunetti BG, Candori P, Falcinelli S, Teixidor MM, Pirani F, Richter R, Stranges S, Vecchiocattivi F (2004) Low-lying electronic states of HBr^{2+}. J Chem Phys 120:6985–6991
40. Magnasco V, Ottonelli M (1999) Dipole polarizability pseudospectra and C6 dispersion coefficients for $H_2{}^+$–$H_2{}^+$. J Mol Struct Theochem 469:31–40
41. Gorfinkiel JD, Tennyson J (2004) Electron–$H_3{}^+$ collisions at intermediate energies. J Phys B: At Mol Opt Phys 37:L343
42. Pluta T, Sadlej AJ, Bartlett R (1988) Polarizability of OH^-. Chem Phys Lett 143:91–96
43. McDaniel EW, Mason EA (1973) The mobility and diffusion of ions in gases. John Wiley, New York
44. Maroulis G (1988) Electrical properties for HCO^+ and NNH^+ from fourthorder Moller-Plesset pertubation theory. Z Naturforsch 43:419–429
45. Chipot C, Dehez F, Angyan J, Millot C, Orozco M, Luque FJ (2001) Alternative approaches for the calculation of induction energies: Characterization, effectiveness, and pitfalls. J Phys Chem A 105:11505–11514
46. Bruno D, Catalfamo C, Capitelli M, Colonna G, Pascale ODE, Diomede P, Gorse C, Laricchiuta A, Longo S, Giordano D, Pirani F (2010) Transport properties of high-temperature Jupiter atmosphere components. Phys Plasmas 17:112315
47. Krstic PS, Schultz DR (1999) Elastic scattering and charge transfer in slow collisions: isotopes of H and H^+ colliding with isotopes of H and with He. J Phys B: At Mol Opt Phys 32:3485–3509
48. Yevseyev AV, Radtsig AA, Smirnov BM (1982) The asymptotic theory of resonance charge exchange between diatomics. J Phys B: At Mol Phys 15:4437–4452
49. Huels MA, Champion RL, Doverspike LD, Wang YC (1990) Charge transfer and electron detachment for collisions of H^- and D^- with H. Phys Rev A 41:4809–4815
50. Copeland FBM, Crothers DSF (1997) Cross sections for resonant charge transfer between atoms and their positive ions atomic data. Nucl Data Tables 65:273–288
51. Roche AE, Goodyear CC (1971) Electron transfer in collisions of low-energy negative oxygen ions with O_2. J Phys D Appl Phys 4:1513–1519
52. Rutherford JA, Vroom DA (1974) The reaction of atomic oxygen with several atmospheric ions. J Chem Phys 61:2514–2519
53. Rapp D, Francis WE (1962) Charge-exchange between gaseous ions and atoms. J Chem Phys 37:2631–2645
54. Brunger MJ, Buckman BSJ (2002) Electron-molecule scattering cross-sections. I. Experimental techniques and data for diatomic molecules. Phys Rep 357:215–458
55. England JP, Elford MT, Crompton RW (1988) A study of the vibrational excitation of H_2 by measurements of the drift velocity of electrons in H_2–Ne mixtures. J Phys 4:573–586
56. Muse J, Silva H, Lopes MCA, Khakoo MA (2008) Low energy elastic scattering of electrons from H_2 and N_2. J Phys B: At Mol Opt Phys 41:095203
57. Shyn TW, Sharp WE (1981) Angular distributions of electrons elastically scattered from H_2. Phys Rev A 24:1734–1740
58. Itikawa Y (1974) Momentum-transfer cross sections for electron collisions with atoms and molecules. Atom Data Nucl Data Tables 14:1–10
59. Bray I, Konovalov DA, McCarthy IE (1991) Coupled-channel optical calculation of electron-hydrogen scattering: elastic scattering from 0.5 to 30 eV. Phys Rev A 43:5878–5885

60. Gupta GP, Mathur KC (1980) Differential cross sections for the elastic scattering of electrons by hydrogen atoms at intermediate energies. J Phys B 13:1719
61. Itikawa Y (2009) Cross sections for electron collisions with oxygen molecules. J Phys Chem Ref Data 38:1–20
62. Sullivan JP, Gibson JC, Gulley RG, Buckman SJ (1995) Low energy electron scattering from O_2. J Phys B 28:4319–4328
63. Linert I, King GC, Zubek M (2004) Measurements of differential cross sections for elastic electron scattering in the backward direction by molecular oxygen. J Phys B 37:468–491
64. Machado LE, Ribeiro EMS, Lee MT, Fujimoto MM, Brescansin LM (1999) Cross sections and polarization fractions for elastic e–O2 collisions. Phys Rev A 60:1199–1205
65. Tabata T, Shirai T, Sataka M, Kubo HA (2006) Analytic cross sections for electron impact collisions with nitrogen molecules. Atom Data Nucl Data Tables 92:375–406
66. Thomas LD, Nesbet RK (1975) Addendum: low energy electron scattering by atomic oxygen. Phys Rev A 12:1729–1730
67. Blaha M, Davis J (1975) Elastic scattering of electrons by oxygen and nitrogen at intermediate energies. Phys Rev A 12:2319–2324
68. Itikawa Y, Ichimura A (1990) Cross sections for collisions of electrons and photons with atomic oxygen. J Phys Chem Ref Data 19:637–651
69. Sobrinho AMC (2004) Elastic and absorption cross sections for electron–hydroxyl radical collisions. Phys Rev A 70:032717
70. Chen X, Morgan LA (1997) Low-energy electron scattering from the X 2Σ state of the OH molecule. J Phys B 30:3709–3717
71. Khakoo MA, Silva H, Muse J, Lopes MCA, Winstead C, McKoy V (2008) Electron scattering from H_2O: elastic scattering. Phys Rev A 78:052710
72. Faure A, Gorfinkiel JD, Tennyson J (2004) Low-energy electron collisions with water: elastic and rotationally inelastic scattering. J Phys B: At Mol Opt Phys 37:801–807
73. Katase A, Ishibashi K, Matsumoto Y, Sakae T, Maezono S, Murakami E, Watanabe K, Maki H (1986) Elastic scattering of electrons by water molecules over the range 100–1000 eV. J Phys B: At Mol Phys 19:2715–2734
74. Itikawa Y (2005) Cross sections for electron collisions with water molecules. J Phys Chem Ref Data 34:1–22
75. Gibson JC, Green MA, Trantham KW, Buckman SJ, Teubner PJO, Brunger MJ (1998) Elastic electron scattering from CO_2. J Phys B: At Mol Opt Phys 32:213–233
76. Iga I, Homem MGP, Mazon KT, Lee MT (1999) Elastic and total cross sections for electron–carbon dioxide collisions in the intermediate energy range. J Phys B: At Mol Opt Phys 32:4373–4388
77. Itikawa Y (2002) Cross sections for electron collisions with carbon dioxide. J Phys Chem Ref Data 31:749–767
78. Gibson JC, Morganz LA, Gulleyx RJ, Brungerk MJ, Bundschuy CT, Buckmany SJ (1996) Low energy electron scattering from CO: absolute cross section measurements and R-matrix calculations. J Phys B: At Mol Opt Phys 29:3197–3214
79. Allan M (2010) Electron collisions with CO: elastic and vibrational excitation cross sections. Phys Rev A 81:042706
80. Lee MT, Iga I, Brescansin LM, Machado LE, Machado FBC (2002) Theoretical studies on electron-carbon monoxide collisions in the low and intermediate energy range. J Mol Struct (Theochem) 585:181–187
81. Land JE (1978) Electron scattering cross sections for momentum transfer and inelastic excitation in carbon monoxide. J App Phys 49:5716–5721
82. Lee MT, Iga I, Machado LE, Brescansin LM (2000) Model absorption potential for electron-molecule scattering in the intermediate-energy range. Phys Rev A 62:062710
83. Cho H, Park YS, Castro EAY, De Souza GLC, Iga I, Machado LE, Brescansin LM, Lee MT (2008) A comparative experimental–theoretical study on elastic electron scattering by methane. J Phys B: At Mol Opt Phys 41:045203
84. Bundschuy CT, Gibsony JC, Gulleyz RJ, Brungerx MJ, Buckmany SJ, Sannak N, Gianturco FA (1997) Low-energy electron scattering from methane. J Phys B: At Mol Opt Phys 30:2239–2259
85. Sohn W, Kochem KH, Scheuerlein KM, Jung K, Ehrhardt H (1986) Elastic electron scattering from CH_4, for collision energies between 0.2 and 5 eV. J Phys B: At Mol Phys 19:3625–3632
86. Nakamura Y (2010) Electron swarm parameters in pure C_2H_2 and in C_2H_2–Ar mixtures and electron collision cross sections for the C_2H_2 molecule. J Phys D Appl Phys 43:365201
87. Khakoot MA, Jayawee T, Wangs S, Trajmarg S (1999) Differential electron scattering from acetylene-elastic scattering and vibrational excitation. J Phys B: At Mol Opt Phys 26:4845–4860

88. Kochem KH, Sohn W, Jung K, Ehrhardt H, Changt ES (1985) Direct and resonant vibrational excitation of C_2H_2 by electron impact from 0 to 3.6 eV. J Phys B: At Mol Opt Phys 18:1253–1266
89. Iga I, Lee MT, Rawat P, Brescansin LM, Machado LE (2004) Elastic and total cross-sections for electron scattering by acetylene in the intermediate energy range. Eur Phys J D 31:45–51
90. Lee MT, Machado LE, Brescansin LM, Iga I (2005) A theoretical study on elastic electron–CHx (x = 1, 2, 3, 4) collisions in the low-energy range. J Phys B: At Mol Opt Phys 38:3795–3804
91. Castroa EAY, Souzab GLC, Brescansind LM, Machadoc LE, Dos Santosc AS, Lee MT (2010) Application of the scaled quasi-free scattering model absorption potential to electron scattering by CHx (x = 1, 2, 3,4). J Electron Spectros Relat Phenom 182:4–10
92. Michelin SE, Oliveira HL, Kroin T, Soares LSS, Veiteinheimer E, Luz CAR, Lima MF, Fujimoto MM, Lee MT (2005) A comparative study for elastic electron collisions on the isoelectronic CNN, NCN, and CCO radicals. J Chem Phys 122:094309
93. Andr′e P, Brunet L, Bussi'ere W, Caillard J, Lombard JM, Picard JP (2004) Transport coefficients of plasmas consisting of insulator vapours. Eur Phys J Appl Phys 25:169–182
94. Fujimoto MM, Lee MT, Michelin SE (2004) Elastic cross sections for electron-ketenylidene (C_2O) collisions. Phys Rev A 69:052706
95. Spencer FE, Phelps AV (1976) Momentum transfer cross sections and conductivity integrals for gases of MHD interest. In: Proceedings of 15th symposium engineering aspects of MHD, University of Pennsylvania, Philadelphia, PA, p IX.9.1
96. Kovitya P (1984) Thermodynamic and transport properties of ablated vapours of PTFE, alumina, perspex and PVC in the temperature range 5000–30000 K. IEEE Trans Plasma Sci 12:38–42
97. Mason EA, Munn RJ (1967) Transport coefficients of ionized gases. Phys Fluids 10:1827–1832
98. Devoto RS (1973) Transport properties of ionized gas. Phys Fluids 16:616–623
99. Murphy AB (2000) Transport coefficients of hydrogen and argon–hydrogen plasmas. Plasma Chem Plasma Process 20:279–297
100. Wright MJ, Hwang HH, Schwenke DW (2007) Recommended collision integrals for transport property computations part 2: Mars and Venus entries. AIAA J 45:281–288
101. Krěnek P (2008) Thermophysical Properties of H_2O–Ar Plasmas at Temperatures 400–50,000 K and Pressure 0.1 MPa. Plasma Chem Plasma Process 28:107–122
102. Magin T, Sdegrze G, Sokolova I (2002) Thermodynamic and transport properties of Martian atmosphere for space entry application 33rd plasmadynamics and lasers conference. Hawaii, 20–23 May 2002